Roughness Based Crossflow Transition Control for a Swept Airfoil Design Relevant to Subsonic Transports

Fei Li[1], Meelan Choudhari[2], Mark Carpenter[3], Mujeeb Malik[4], Chau-Lyan Chang[5] and Craig Streett[6]
Computational AeroSciences Branch, NASA Langley Research Center, Hampton, VA 23681

Abstract

A high fidelity transition prediction methodology has been applied to a swept airfoil design at a Mach number of 0.75 and chord Reynolds number of approximately 17 million, with the dual goal of an assessment of the design for the implementation and testing of roughness based crossflow transition control and continued maturation of such methodology in the context of realistic aerodynamic configurations. Roughness based transition control involves controlled seeding of suitable, subdominant crossflow modes in order to weaken the growth of naturally occurring, linearly more unstable instability modes via a nonlinear modification of the mean boundary layer profiles. Therefore, a synthesis of receptivity, linear and nonlinear growth of crossflow disturbances, and high-frequency secondary instabilities becomes desirable to model this form of control. Because experimental data is currently unavailable for passive crossflow transition control for such high Reynolds number configurations, a holistic computational approach is used to assess the feasibility of roughness based control methodology. Potential challenges inherent to this control application as well as associated difficulties in modeling this form of control in a computational setting are highlighted. At high Reynolds numbers, a broad spectrum of stationary crossflow disturbances amplify and, while it may be possible to control a specific target mode using Discrete Roughness Elements (DREs), nonlinear interaction between the control and target modes may yield strong amplification of the difference mode that could have an adverse impact on the transition delay using spanwise periodic roughness elements.

Nomenclature

A_{init}	=	initial amplitude of crossflow instability mode or secondary instability mode
C, c	=	wing chord length measured in direction perpendicular to leading edge
f	=	frequency of instability oscillations
M	=	freestream Mach number
N	=	N-factor of linear crossflow instability or secondary instability
Re_c	=	Reynolds number based on wing chord
X, x	=	chordwise coordinate in direction perpendicular to leading edge
Y	=	wall-normal coordinate
Z	=	spanwise coordinate in direction parallel to leading edge
Λ	=	wing sweep angle
λ	=	spanwise wavelength of crossflow instability in millimeters in direction parallel to leading edge

I. Background

Substantial reductions in the fuel burn of future aircraft have been targeted both in the U.S.[1] and in Europe[2] in order to lower the cost of air travel and alleviate the impact of aviation on the environment. A substantial fraction of the targeted reductions in aircraft fuel burn will come from the reductions in vehicle drag. For today's commercial transport aircraft, up to one half of the total drag corresponds to skin friction drag. Because laminar

[1] Aerospace Technologist, MS 128, fei.li@nasa.gov.
[2] Aerospace Technologist, MS 128, meelan.m.choudhari@nasa.gov, Associate Fellow, AIAA.
[3] Aerospace Technologist, MS 128, mark.h.carpenter@nasa.gov.
[4] Aerospace Technologist, MS 128, chau-lyan.chang@nasa.gov, Senior Member, AIAA.
[5] Aerospace Technologist, MS 128, mujeeb.r.malik@nasa.gov, Fellow, AIAA.
[6] Aerospace Technologist, MS 128, craig.l.strreett@nasa.gov.

skin friction is much lower in comparison with the turbulent skin friction, flow control via delayed boundary-layer transition over major aerodynamic surfaces holds the potential to provide the desired reductions in the overall drag.

NASA's Subsonic Fixed Wing Project is investigating several options to help develop robust technology concepts for laminar flow control and to accelerate their insertion into the operational fleet.[1] One of those concepts involves the delay of crossflow-induced transition over a swept aerodynamic surface using control input in the form of appropriately positioned Discrete Roughness Elements (DREs) near the leading edge.[3] A bulk of the existing experimental and computational studies of the DRE concept have been carried out for either incompressible or supersonic configurations with modest wing-chord Reynolds numbers of up to approximately 8 million,[4,5] and with pressure distributions that may not be optimal for wing designs for subsonic transport aircraft flying at Mach numbers between 0.75 to 0.90. Consequently, additional effort is deemed necessary to assess the potential capability of the DRE concept to control swept wing transition at transonic Mach numbers and substantially higher chord Reynolds numbers than previous applications.

Given the sensitivity of transition to wind tunnel disturbances and the cost of flight experiments, computational tools will need to play an important role in the assessment of DREs for subsonic transport vehicles, as a means of risk reduction as well as to help optimize the DRE design. The DRE concept seeks to delay transition via controlled seeding of subdominant crossflow modes that cannot lead to transition on their own, but can keep the naturally dominant instability modes at bay via nonlinear modification of the basic state and/or mode competition. This intrinsically nonlinear control mechanism calls for a higher fidelity prediction approach involving all of the relevant stages of the transition process, namely, receptivity, linear and nonlinear growth of primary crossflow instabilities, and secondary instability.[6] The individual ingredients of this approach have been available for some time and partial integration of those ingredients has been demonstrated in prior works.[6–11] Computations along this line have been performed for the low Mach number configuration of the flight experiment at chord Reynolds numbers of 7 to 8 million.[4,5] The results show that the most unstable stationary crossflow mode is weakened in the presence of roughness elements, with an accompanying reduction in the growth potential of the high-frequency secondary instability modes that are likely to cause the onset of laminar-turbulent transition.[11] However, the same results also indicate that the control mode amplitudes required to stabilize the dominant modes can become excessively large, especially when the maximum N-factors are rather large, so that the possibility of premature transition due to overcontrol cannot be entirely discounted. Similar findings have also been obtained for a supersonic swept wing configuration at Mach 2.4 and chord Reynolds number of 16 million.[12]

In recent work,[13] Texas A & M University has performed a conceptual design study of a Laminar Flow Control (LFC) flight test with target conditions of $M \approx 0.75$, a chord Reynolds number, Re_c, between 15 and 20 million, and a leading-edge sweep angle, Λ, of 30°. The resulting wing has significant potential for natural laminar flow over both suction and pressure surfaces at the design angle-of-attack of 0 degrees. At off-design conditions, however, an earlier transition may occur as a result of stationary crossflow modes, which opens up the possibility of roughness based transition control on the same model, either to increase the lift coefficient or to extend the angle-of-attack range for laminar flow.[13] The broad objectives behind the present effort are to assess the feasibility of achieving DRE based transition control using NASA's prediction tools for receptivity, nonlinear development and secondary instability stages of the transition process and, in doing so, to help mature those prediction tools and the methodology to apply them in a practical context.

II. Flow Configuration and Analysis Codes

The design process for the laminar flow airfoil TAMU-003T-75(v.90) has been described in ref. 13 and also reported in a companion paper.[14] In brief, the 9.3 percent thick, 30-degree swept airfoil is designed to achieve natural laminar flow over 60 and 50 percent of the suction and pressure surfaces, respectively, at the design condition of zero degree angle of attack, Mach number of M = 0.75, and chord Reynolds number of approximately 17 million based on free-stream speed, a streamwise chord length of 12 ft, and free-stream temperature of 390 R, corresponding to a flight altitude of 40,000 ft. Design constraints for the wing included (i) a lift coefficient that is typical of subsonic transports, and (ii) a wing thickness distribution that is suitable for a mid-size business jet. Both Tollmien-Schlichting and crossflow instabilities are sufficiently weak at the design angle of attack, so that natural laminar flow should be achievable over a significant portion of the airfoil surface ($x/c>0.6$ on suction surface and $x/c>0.5$ on the pressure side) without any external means of boundary layer control. In this paper, we focus on the off design condition corresponding to an angle of incidence equal to -1 degree. At this condition, a stronger

crossflow instability exists along the suction side[13,14] and, hence, could provide a potential means to assess DRE based laminar flow technology at higher Reynolds numbers than previous tests.

For the work described in this paper, the mean boundary-layer flow over the suction surface of the airfoil is computed with a boundary layer solver[15] using the infinite span approximation, in conjunction with the inviscid surface pressure distribution derived from an Euler solution under free flight conditions.[13-14] Linear and nonlinear development of the instability modes is computed using parabolized stability equations (PSE) as implemented in the Langley Stability and Transition Analysis Codes (LASTRAC).[16] The growth of high frequency secondary instability modes supported by the finite amplitude stationary crossflow vortex is analyzed in a manner similar to the classical linear stability analysis of swept airfoil boundary layers. Details of the methodology employed for secondary instability predictions may be obtained from Ref. 10. The main difference between the primary and secondary stability analyses is that the basic state for the secondary modes (i.e., the mean boundary layer flow modified by the primary crossflow mode) varies in both surface normal and spanwise directions and, hence, the instability characteristics of the secondary modes must be analyzed using a planar, partial differential equation based eigenvalue problem, rather than as an ordinary differential equation based eigenvalue problem for the classical analysis. The selection of grid and other aspects of the numerical solution was based on extensive experience with similar class of flows,[6,7,9,10,11] and spot checks were made to ensure that the impact of reasonable variations with respect to those choices was negligible. Typically, 121 points in the wall-normal direction and 33 points in the spanwise direction are used for the 2D eigenvalue analysis. For nonlinear PSE marching, 281 points are used in the wall-normal direction (which is more than sufficient), and the streamwise marching step-size is appropriately adjusted for each case, if necessary, in order to to capture the corresponding modal evolution.

III. Crossflow Transition in the Absence of Control Input

A. Linear Amplification Factors

Earlier experiments at the Texas A & M University[3,4] have shown that crossflow transition in a flight disturbance environment is dominated by stationary crossflow instabilities, despite the lower amplification factors of stationary modes relative to the non-stationary (i.e., traveling) crossflow modes. For the present a wing configuration, the stationary crossflow vortices that achieve the highest linear amplification at the off design condition of interest correspond to a spanwise wavelength of approximately 8 mm.[13,14] Streamwise evolution of logarithmic amplification ratios (N-factors) corresponding to a range of spanwise wavelengths is shown in Fig. 1. Observe that stationary modes over a broad range of spanwise wavelengths ($\lambda \approx 4$ mm to $\lambda = 17$ mm) attain a peak linear N-factor of greater than 8. Therefore, based on linear stability correlations,[3] all of those modes possess the potential to cause transition on their own. In fact, the shorter wavelengths such as $\lambda = 6$ mm achieve their peak amplitudes upstream of the 8 mm mode and, hence, could become the dominant cause for transition.

Of course, whether or not transition will occur in any given case and, if it does, then which stationary mode will dominate the transition process is determined by a combination of factors such as the effective initial amplitudes of relevant stationary modes, their linear and nonlinear amplification characteristics and the growth of high frequency secondary instabilities after the vortices have attained finite amplitudes. The initial amplitudes are mainly determined by the roughness characteristics of the airfoil surface and large variations in the transition onset location are known to result from changes in surface finish, especially near the wing leading edge.[3-4] A combination of receptivity analysis, along with suitable assumptions regarding the statistical characteristics of surface roughness, can be used to estimate the range of amplitudes of stationary crossflow instabilities excited due to naturally occurring surface roughness. An analysis of this type was used in Ref. 17 to help explain the dramatic effect of leading edge surface finish on the observed transition location during the low-speed Swept Wing Flight Test (SWIFT) by Texas A & M University.[3-4] However, an extension of that analysis to the present wing configuration has not been completed. Consequently, the choice of initial amplitudes in the present paper is somewhat arbitrary, but guided by the results of Ref. 17.

B. Nonlinear Development of Individual Stationary Modes

To gain some insight into the nonlinear evolution of individual stationary modes, nonlinear PSE computations were performed for selected values of spanwise wavelength and specified initial amplitudes. In Figs. 2(a)-2(c), the amplitude of the fundamental spanwise harmonic corresponding to each selected mode is plotted as a function of the (normalized) chordwise coordinate x/c for three values of initial amplitude. Based on previous analysis[11] for the

SWIFT flight experiments, this range of initial amplitudes is believed to be representative of the aerodynamic surfaces encountered in laminar flow applications. Here the initial amplitude is measured in terms of the maximum chordwise perturbation velocity normalized by the freestream velocity.

A comparison of the results from Figs. 1 and 2 shows that, with finite initial amplitudes, the region of growth in fundamental amplitude becomes smaller than the range of unstable locations based on linear PSE. Thus, with an increasing initial amplitude, the location of peak disturbance amplitude moves progressively, albeit slowly, forward relative to the downstream branch of the neutral curve based on linear theory. At the smallest initial amplitude (or, equivalently, a relatively smooth airfoil surface), only the $\lambda = 8$ mm mode achieves large enough amplitudes that are likely to induce a strong secondary instability and, hence, the onset of transition. (Results of secondary instability analysis for this case are described further below in this section.) As the initial amplitude increases to 0.0001, stationary crossflow modes with wavelengths between $\lambda = 6$ mm and $\lambda = 12$ mm attain fundamental amplitudes in excess of 0.20 and, due to its earlier growth, the 6 mm mode could well be the dominant culprit for transition. At the highest initial amplitude considered in this figure (Fig. 2(c)), there appears little question about the ability of the 6 mm mode to sustain a strong enough secondary instability growth to initiate transition. In fact, even the $\lambda = 4$ mm mode has achieved significantly large amplitudes to become a potential cause for transition in this case. At all three values of the initial amplitude parameter, however, the 2.67 mm stationary mode remains too weak to become a vehicle for transition onset. Thus, it appears to be well suited as a control input with higher initial amplitudes.

C. Linear Amplification of High-Frequency Secondary Instabilities

A secondary instability analysis provides greater insights into whether or not the nonlinear amplitudes observed in Fig. 2 can lead to transition. A thorough analysis of this type was not possible within the duration of this study and, hence, two specific wavelengths ($\lambda = 8$ mm and $\lambda = 2.667$mm) were selected to address the onset and amplification of secondary instabilities. Further details on the procedure used for the secondary instability analysis may be found in Ref. 10.

For the linearly dominant stationary crossflow mode with 8 mm wavelength, the initial amplitude was set equal to 0.00001. This value is roughly consistent with the range of initial crossflow amplitudes associated with relatively smooth aerodynamic surfaces, as inferred from a similar analysis of an earlier set of flight experiments.[11,17] The same integrated approach combining predictions for receptivity, linear and nonlinear amplification of primary instabilities (i.e., stationary crossflow vortices) and resulting evolution of secondary crossflow modes may now be used to estimate the transition onset location for the present wing design.

The finite amplitude stationary crossflow vortex 8 mm target mode supports multiple families of secondary instability modes. Mode shapes corresponding to four of the most dominant families of secondary instability modes are shown in Fig. 3. For convenience, these are termed as modes 1 through 4, respectively; however, the ordering of the mode families is rather arbitrary. Modes 1 and 3 are the so called “Y-modes” in the terminology of Ref. 7, while modes 2 and 4 are “Z-modes”.

The range of frequencies spanned by the various families of secondary instability modes at $x/c = 0.485$ is shown in the top half of Fig. 4. The most unstable mode (Mode 1) is centered at a frequency of approximately 60 kHz. The spatial amplification characteristics of various fixed frequency disturbances belonging to each of these four families are shown in the bottom half of Fig. 5. Both Y-modes reach very high secondary N-factors, while the Z-mode secondary N-factors are below 7.

The 2.67 mm mode, which has a linear N factor of approximately 6 and, hence, is suitable as a control input based on DREs, is also susceptible to secondary instability if the initial amplitude becomes sufficiently large. The mode shapes of three dominant families of secondary instability modes, for an initial primary amplitude of 0.01, are shown in Fig. 5. This large initial amplitude is chosen somewhat arbitrarily to sustain strong secondary instability. These are again numbered mode 1, 2 and 3. In this case, modes 1 and 2 are Y-modes and mode 3 is a Z-mode. Spatial amplification characteristics of the 2.67 mm control mode are shown in Figure 6. The most amplified secondary mode is mode 1, i.e., a Y-mode. The maximum secondary N-factor is less than 8. Therefore, if one assumes that the transition onset based on linear amplification of secondary instabilities correlates with an N-factor of greater than 8 (i.e., corresponds to the same approximate range as that for primary instabilities), then transition would be just avoided in this case. It should be noted that Ref. 19 raised some questions regarding whether or not the Y-mode instabilities are realizable even in theory. However, the linear and nonlinear PSE analysis in Ref. 11

and that described in section IV below indicates that, if the Y-modes can get excited in a given flow, then they would achieve a considerable spatial growth and, indeed, can lead to transition under appropriate circumstances. In view of those findings, the main issue regarding the realizability of the Y-modes would appear to involve the excitation (i.e., receptivity) mechanisms for these modes in a given disturbance environment.

IV. Nonlinear Evolution and Breakdown of Secondary Instability

As described in Ref. 11, the linear predictions of secondary instability may be used for transition onset correlation using a secondary N-factor criterion. However, it is also instructive to study the nonlinear evolution of the secondary mode perturbations in order to understand the breakdown mechanisms responsible for the onset of transition. Wassermann and Kloker[20] carried out direct numerical simulations (DNS) of secondary instability well into the breakdown region and revealed some interesting features of the breakdown process for a specific wind tunnel configuration. Although DNS is a powerful tool, it is also costly. The present section investigates the application of nonlinear parabolized stability equations (PSE) to capture the initial portion of the breakdown process at a computational cost that is at least an order of magnitude lower in comparison with the DNS. Illustrative PSE computations of the breakdown of crossflow vortices with $\lambda = 8$ mm via the secondary instability mechanism are presented below.

The secondary instability eigenfunction is computed very close to the neutral point predicted by the linear, PDE based eigenvalue analysis, and is used to initiate the nonlinear PSE computation involving both the primary (i.e., stationary crossflow) and secondary modes. Figure 7 shows the comparison between the root-mean-square (RMS) amplitudes of the secondary instability modes as derived from the nonlinear PSE and the linear secondary instability theory, respectively. The left half of Fig. 7 shows the evolution of a Y-mode of secondary instability at the frequency of f = 62.5 kHz, whereas the right half shows similar comparison for a Z-mode at f = 42.5 kHz, each of these frequencies corresponds to the most amplified frequency of the respective mode. The red, green and blue lines represent, respectively, the RMS amplitudes of secondary instability modes with initial amplitudes of 10^{-6}, 10^{-4} and 10^{-2}. These amplitudes have been normalized with their respective initial amplitudes so that they collapse onto each other, initially. As the instabilities grow, these curves depart from each other due to nonlinear effects. The black dots in Fig. 7 represent predictions based on the linear secondary instability theory, which have been shifted vertically to match the PSE results in the linear (small amplitude) portion of the secondary evolution. Fig. 7(a) shows that there is some initial discrepancy between the linear theory and PSE results for the Y-mode. The reason for this is currently unclear, but the PSE solution is known for having initial transient behavior when the inflow condition deviates from the relevant non-parallel eigensolution. In any case, after the transient dies out, the PSE solution agrees very well with the secondary instability theory. On the other hand, for the Z-mode shown in Fig.7(b), there is good agreement between the linear secondary instability theory and PSE evolution across the entire region until just before the onset of transition (see Fig. 9 below) due to nonlinear breakdown of the secondary instability modes.

Figure 8 shows the modal amplitudes of stationary crossflow vortices and secondary instability at different spanwise wave numbers as obtained from the PSE computations, with an initial stationary crossflow vortex amplitude of 10^{-5} and a secondary instability initial amplitude of 10^{-6} respective neutral points. The red and green lines indicate the modal amplitudes of, respectively, stationary crossflow modes and high frequency secondary modes. The black dots represent the linear growth predictions based on the secondary instability theory. Agreements between PSE and secondary instability are similar to those in Fig. 7.

Figure 9 displays the streamwise development of wall shear averaged in time and spanwise coordinate. The onset of transition is characterized by a rise in wall-shear. It is interesting to note that, with the Z-mode evolution (Fig. 9b), the mean wall shear actually undershoots before displaying the rapid rise representative of transition onset. The undershoot in wall shear is associated with a local lift up of low speed fluid from the wall just below the location of intense high frequency oscillations. Because it was not seen during the earlier computations for a different swept wing configuration,[11] it appears to be a configuration dependent feature of transition via Z-modes of secondary instability.

Figure 10 indicates the cross-plane distributions of the RMS perturbation associated with the high frequency instability at selected chordwise locations. At each station, the amplitude distribution is normalized to have a maximum value of unity. For small values of x/c, the amplitude distributions mimic the linear eigenfunctions shown in Fig. 3 and retain that characteristic over much of the region between the onset of secondary instability and where

the transition onset occurs as reflected via the sharp rise in spanwise averaged wall shear. Farther downstream, the amplitude distributions become more spread, affecting a larger cross-sectional area..

V. Stationary Crossflow Vortices and Effect of Control

A. Control of 8 mm mode via control input at λ = 2.67 mm

Having examined the transition characteristics associated with isolated stationary modes, the control of more unstable modes via comparatively benign modes with larger initial amplitudes (seeded via DREs at the appropriate wavelength) is addressed next. The control of the 8 mm wave, referred to as the target mode hereafter, by the λ = 2.67 mm mode (i.e., the control input) is analyzed first. The λ = 2.67 mm mode begins to amplify very close to the leading edge but ceases its growth near approximately 8 percent of the wing chord. In fact, its subsequent decay is strong enough that the linear N-factor drops to zero at approximately 20 percent of the chord. A short amplification range of this type is a desirable feature for the control mode, since that makes it unlikely to reach large enough amplitudes to trigger transition on its own. Of course, the short range of amplification also limits the control action of this mode to a relatively short distance and the possibility of multi-stage control may need to be considered in order to sustain the control action over a longer distance.[6]

Now, the control scenario is considered. The λ = 2.67 mm mode with a larger initial amplitude is introduced as the control input for its more unstable subharmonic with λ = 8 mm. For computations involving more than one mode, the initial amplitude is measured at the neutral location corresponding to the longer wavelength (i.e., 8 mm) mode, i.e., slightly downstream of the neutral location for the shorter wavelength mode(s). Results pertaining to the combined nonlinear evolution of the dominant crossflow mode with an initial amplitude of 10^{-5} and the control mode with a range of the initial amplitudes are described first (Fig. 11). In the absence of any control, the target mode achieves rather high amplitudes, exceeding 30 percent of the free-stream speed as indicated by the solid red curve in Fig. 11. As described in the previous section, these values of uncontrolled amplitudes are more than sufficient to initiate transition via secondary instabilities. However, as the control amplitude is increased progressively, the target amplitude is reduced in a monotonic fashion. Figure 12 illustrates a typical sequence of velocity contours for initial control mode amplitude of 10^{-2}. It provides a visual confirmation that the control mode dominates the disturbance behavior at upstream locations, but eventually yields to the 8 mm vortices downstream.

The nonlinear PSE computations above demonstrate that the control input via the λ = 2.67 mm mode can successfully reduce the amplification of the target stationary modes at λ = 8 mm. To gain insights into the extent of resulting delay in the onset of transition, the secondary instability characteristics in the presence of control input with various magnitudes are analyzed next. The reduction in target mode amplitude with increasing control input results in a progressive reduction in the associated N-factors for secondary waves, as seen from the right portion of Fig. 13. If the transition onset location is assumed to correlate with a secondary N-factor of, say, 9, then an initial control mode amplitude of 5×10^{-3} will push the transition front downstream by approximately 10 percent of the chord (see Fig. 14, which combines the results for primary evolution from Fig. 11 with the transition locations estimated from Fig. 9). Based on previous experimental measurements for the NLF-0415(b) airfoil,[18] it is expected that a further increase in the control amplitude up to approximately 10^{-2} would extend the onset of transition significantly beyond the suction peak location near 67 percent chord, without incurring the danger of overcontrol.

The effect of the initial phase difference between the target and control modes was also examined in brief and, in this particular case, the computations revealed little sensitivity of the primary mode evolution in the downstream region. Additional computations were performed to investigate the effect of higher initial amplitude of the target mode (or, equivalently, the effect of higher amplitude background surface roughness). Figure 15 shows the evolution of the target mode amplitude for the same control inputs as Fig. 11, but for target modes with an initial amplitude of 10^{-4}. Even though the control input is unable to reduce the peak target mode amplitudes in this case, those amplitudes are attained significantly farther downstream in the presence of the control input, suggesting a comparable benefit in terms of incremental transition delay as that for the lower target mode amplitudes (Fig 11).

B. Control of other unstable modes via control input at λ = 2.67 mm

Recall from Figs. 1 and 2 that one of the challenges in implementing DRE based control at higher Reynolds numbers corresponds to the increasingly broader spectrum of stationary crossflow modes that can lead to transition. For example, stationary modes over the range of approximately λ = 4 mm to λ = 17 mm achieve linear N-factors of 8 or above. Thus, it is also important to determine if the λ = 2.67 mm mode can suppress the growth of crossflow

instabilities throughout that range. To investigate this question, the evolution of 4 mm and 13.33 mm modes in the presence of the λ = 2.67 mm control input was examined computationally. The initial amplitude of these target modes was assumed to be 10^{-5}, i.e., the same as that of the 8 mm mode in Fig. 11. Although not shown, the λ = 2.67 mm mode was found to be effective in reducing the growth of the long wavelength mode (λ = 13.33 mm). On the other hand, there was less delay in growth for the 4 mm mode (Fig. 16) than the corresponding delay for the more unstable, 8 mm target mode. Much more importantly, although the 8 mm mode is not initiated on input, the nonlinear interaction (*i.e.* difference interaction) between the control and target modes leads to strong excitation of the 8 mm mode (solid dots in Fig. 16), which achieves the same level of amplitudes within the mid chord region as the same mode in the absence of any control. However, the effective amplitude of the 8 mm mode decreases with increasing control input, enabling the rise of 8 mm mode to be counteracted via increased control input.

The strong excitation of long wavelength modes via nearly tuned nonlinear interactions between two shorter wavelength modes was also noted in previous work related to a supersonic swept wing configuration[6,10] and, hence, appears to be a common phenomenon.

C. Use of λ = 4 mm mode as control input

Because the λ = 4 mm mode corresponds to the first harmonic of the most amplified 8 mm mode, using the former as the control input may mitigate some of the issues related to the strong excitation of the longer wavelength modes via difference interactions with the dominant target modes. On the other hand, this mode leads to higher peak amplitudes than those of the 2.67 mm mode (recall Fig. 2) and, hence, has a higher chance of leading to premature transition due to excessive control input. The control of λ = 8 mm and λ = 6 mm modes via increasing amplitudes of the λ = 4 mm mode was considered next (Figs. 17(a) and 17(b), respectively). In the 8 mm case, a modest control input corresponding to an initial amplitude of 10^{-3} can practically eliminate the target mode from being a dominant factor in transition - there is no strong nonlinear excitation and growth of additional crossflow modes - and the potential for overcontrol appears marginal. On the other hand, interaction of the 4 mm mode with the 6 mm target mode leads to near resonant excitation of the longer wavelength 12 mm mode, similar to when the 2.67 mm control input was used in conjunction with target mode with λ = 8 mm. The control input with an initial amplitude of 0.001 is no longer sufficient to keep the 12 mm mode at reasonably low amplitudes. While higher values of the control input are effective in controlling both λ = 6 mm and λ = 12 mm modes, they are accompanied by a higher potential for overcontrol by virtue of the higher peak amplitudes of the 4 mm mode. This difficulty is exacerbated when the target mode amplitudes are larger, as seen from Fig. 18.

VI. Summary

This ongoing effort targets the development, application, and improvement of higher fidelity tools for DRE based laminar flow control over subsonic/transonic aircraft. The results illustrate that useful insights may be gained into the efficacy and/or optimization of a given DRE application using such tools in the desired Mach and Reynolds number regimes. Specifically, holistic predictions of this type, which integrate the knowledge of receptivity, linear and nonlinear amplification of primary crossflow instabilitiy and the high-frequency secondary instabilities, can provide the basis for risk reduction studies for costly flight experiments and help ascertain the optimal implementation of DREs over the relevant range of operating conditions.

This paper highlights some of the intrinsic challenges in implementing DRE based laminar flow technology at higher Reynolds numbers relevant to subsonic transport aircraft, along with the associated difficulties in modeling this form of control in a computational setting. Implementing DRE based control at large Reynolds numbers involves a delicate balance between reducing the growth of a broad spectrum of highly amplified stationary crossflow modes and the possibility of premature transition due to excessive control input. While control of dominant modes appears feasible at low enough amplitudes of target modes, the prospects of overcontrol become more likely at higher initial target mode amplitudes (i.e., less smooth leading edge surfaces). Nonlinear interactions between the short wavelength control mode and target modes of comparable wavelength are also worthy of attention because of potentially strong amplification of the difference mode arising from such interactions.

On the modeling side, analysis of interactions between a small number of discrete modes from the relevant band of stationary crossflow wavelengths can provide useful insights into the nature of crossflow instability evolution under various scenarios related to its initial amplitude spectrum. Such analysis can also be extended to include secondary instability computations, permitting estimates for the onset of transition and the extent of delay due to

DREs. However, to enable more reliable predictions, it will be essential to look at the combined evolution of a broadband initial spectrum of stationary crossflow disturbances. Such an approach can be easily coupled with receptivity predictions for natural surface roughness, allowing a stochastic treatment of the overall problem. Computations of DRE based control in the presence of broadband background disturbances have been carried out for the lower Reynolds number NLF-0415(b) configuration in the past, and will be extended to the higher Reynolds configurations of practical interest during future work.

Acknowledgments

The present work is part of a collaborative effort with Prof. W.S. Saric and his research group at Texas A & M University (TAMU). Technical interactions with the TAMU team are gratefully acknowledged. The authors also thank Mr. Michael Belisle from TAMU for providing the design data associated with the wing configuration studied herein. This work was performed in support of NASA's Subsonic Fixed Wing and the Environmentally Responsible Aviation projects.

References

1. Collier, F., "Subsonic Fixed Wing Project Overview," Proceedings of NASA FAP 2008 Annual Meeting, Atlanta, Oct. 7-9, 2008.
2. Report of the Group of Personalities, "European Aeronautics: A Vision for 2020," Office for Official Publications of the European Communities, January 2001.
3. Saric, W. S., Carillo, R. B., and Reibert, M. S., "Leading Edge Roughness as a Transition Control Mechanism," AIAA Paper 98-0781, Jan. 1998.
4. Carpenter, A.L., Saric, W.S., and Reed, H.L., "Laminar Flow Control on a Swept Wing with Distributed Roughness," AIAA Paper 2008-7335, 2008.
5. Rhodes, R.G., Carpenter, A.L., Reed, H.L., and Saric, W., "CFD Analysis of Flight-Test Configuration for LFC on Swept Wings," AIAA Paper 2008-7336, 2008.
6. Choudhari, M., Chang, C.-L., Streett, C. L. and Balakumar, P., "Integrated Transition Prediction: A Case Study in Supersonic Laminar Flow Control," AIAA Paper 2003-0973, 2003.
7. Malik, M.R., Li, F., Choudhari, M., and Chang, C.-L., ``Secondary Instability of Crossflow Vortices and Swept-Wing Boundary-Layer Transition," *J. Fluid Mech.,* Vol. 399, pp. 85-115, 1999.
8. Janke, E., "Receptivity and Transition Control of Swept-Wing Boundary-Layers: Effects of Surface Curvature and Nonlinearity," AIAA Paper 2001-2980, 2001.
9. Chang, C.-L. and Choudhari, M. M., "Boundary-Layer Receptivity and Integrated Transition Prediction," AIAA Paper 2005-0526, 2005.
10. Li, F. and Choudhari, M., "Spatially Developing Secondary Instabilities and Attachment Line Instability in Supersonic Boundary Layers," AIAA Paper 2008-590, 2008.
11. Li, F., Choudhari, M., Chang, C.-L., Streett, C. L. and Carpenter, M. H., "Roughness Based Crossflow Transition Control: A Computational Assessment," AIAA Paper 2009-4105, 2009.
12. Choudhari, M, Chang, C.-L. and Jiang, L., "Towards Transition Modeling for Supersonic Laminar Flow Control," *Philosophical Transactions of Royal Society of London (Physical and Mathematical Sciences)*, vol. 363, no. 1830, pp. 1041-1259, 2005.
13. Saric, W.S., "Flight Experiments on Swept-Wing Roughness Receptivity: Phase 2. Feasibility of a laminar flow flight test," Phase 2, Year 1 Draft Report for AFOSR Grant FA955008-1-0475, June 2, 2009.
14. Belisle, M., Neale, T., Reed, H. and Saric, W. "Design of a Swept-Wing Laminar Flow Control Flight Experiment for Transonic Aircraft," AIAA paper 2010-4381, 2010.
15. Wie, Y.-S., "BLSTA – A Boundary Layer Code for Stability Analysis," NASA CR 4481, 1992.
16. Chang, C.-L., "Langley Stability and Transition Analysis Code (LASTRAC) Version 1.2 User Manual," NASA/TM-2004-213233, June, 2004.
17. Carpenter, M. H., Choudhari, M. M., Li, F., Streett, C. L. and Chang, C.-L., "Excitation of Crossflow Instabilities in a Swept Wing Boundary Layer," AIAA Paper 2010-378, 2010.
18. Carrillo, R. B., Jr, Reibert, M. S. and Saric, W. S. "Distributed Roughness Effects on Stability and Transition in Swept Wing Boundary Layers," Final report for NASA LaRC Co-operative Agreement NCC-1-194, 1996
19. Bonfigli, G, and Kloker, M. "Secondary Instability of Crossflow Vortices: Validation of the Stability Theory by Direct Numerical Simulation," *J. Fluid Mech.*, Vol. 583, pp. 229-272, 2007.
20. Wassermann, P. and Kloker, M., "Mechanisms and Passive Control of Crossflow-Vortex-Induced Transition in a Three-Dimensional Boundary Layer," *J. Fluid Mech.,* Vol. 456, pp.49-84, 2002.
21. Chang, C.-L. and Choudhari, M., "Boundary layer Receptivity and Integrated Transition Prediction," AIAA Paper 2005-526, 2005.

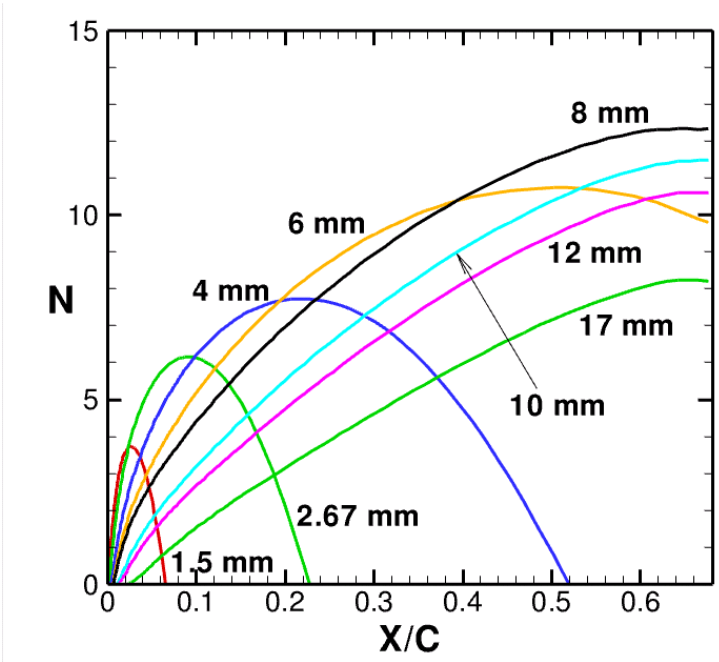

Figure 1. Linear N-factors of primary stationary crossflow vortices of selected spanwise wavelengths.

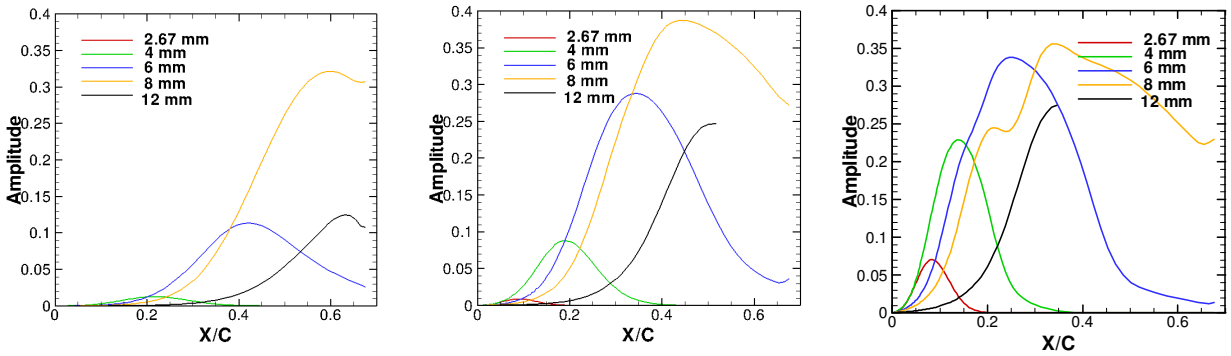

(a) $A_{init} = 10^{-5}$ (b) $A_{init} = 10^{-4}$ (c) $A_{init} = 10^{-3}$

Figure 2. Nonlinear evolution of fundamental disturbance amplitude for stationary crossflow modes with a fixed specified initial amplitude, with the spanwise wavelength as a parameter

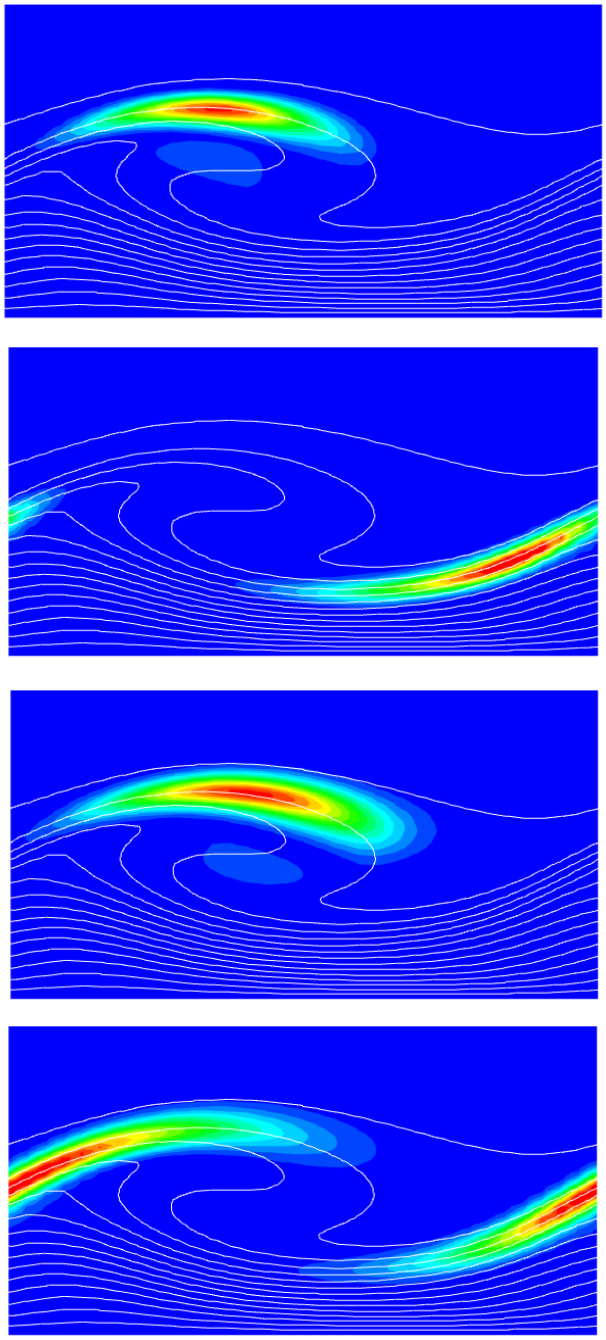

Figure 3. Mode shapes in terms of chordwise velocity fluctuations for four dominant families of 8mm secondary instability modes without any control at x/c = 0.485. From top to bottom: mode 1, 2, 3, and 4, respectively. Thin white lines in the background represent contours of chordwise velocity distribution associated with a finite amplitude crossflow vortex with λ_z = 8 mm.

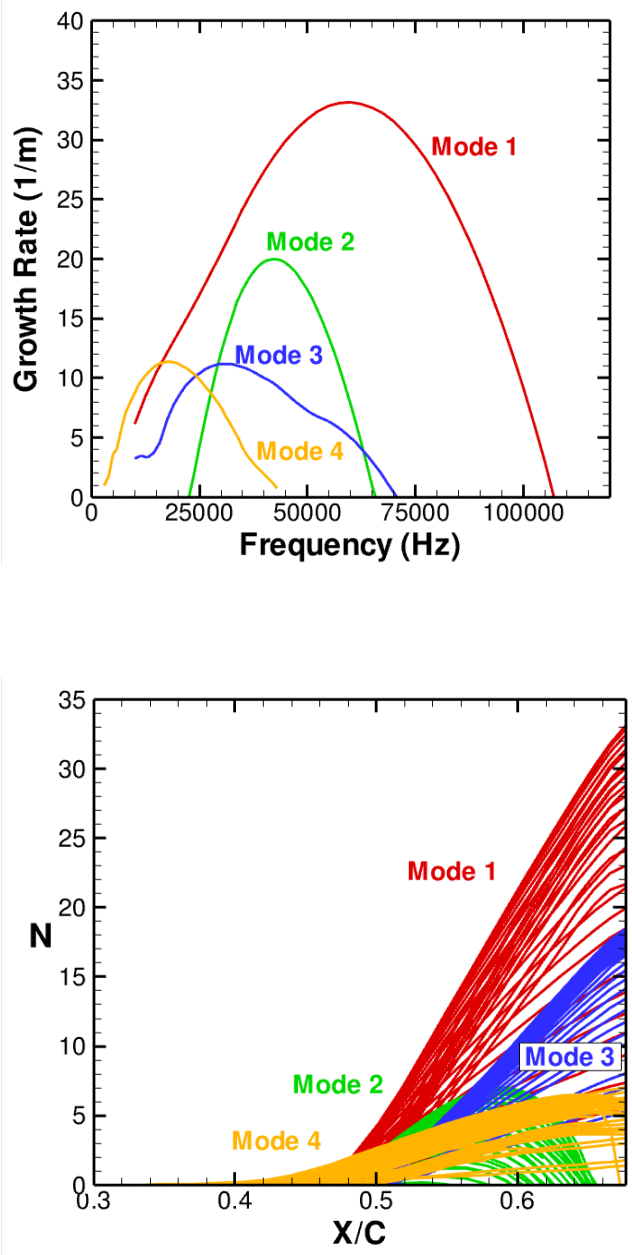

Figure 4. Top: growth rates of the four dominant families of 8mm secondary instability modes at x/c = 0.485 (uncontrolled case). Bottom: secondary N-factor curves associated with constant frequency disturbances belonging to each family. Each curve represents a fixed frequency disturbance and curves of the same color belong to a given family.

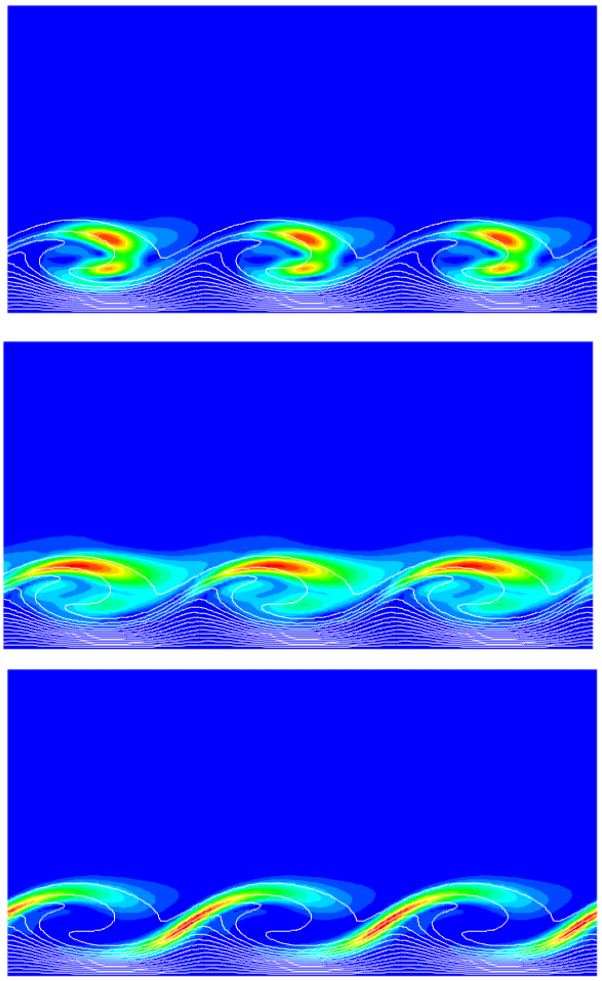

Figure 5. Mode shapes in terms of chordwise velocity fluctuations of three dominant families of 2.67mm secondary instability modes at x/c = 0.06. From top to bottom, mode 1, 2 and 3. Thin white lines in the background represent baseflow chordwise velocity contours of 2.67mm crossflow vortices. (Length scale is the same as that in Fig. 3)

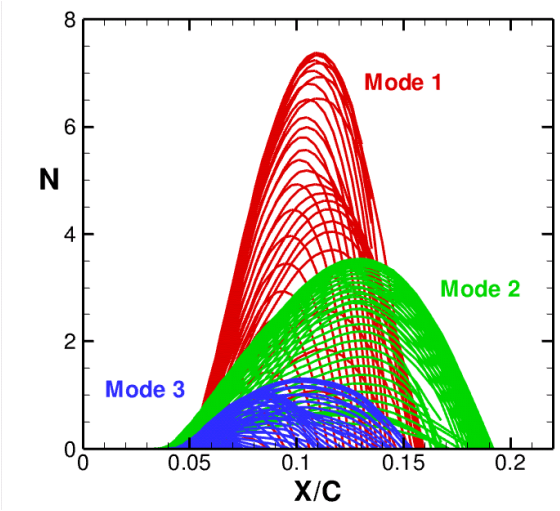

Figure 6. N-factors of the three dominant families of secondary instability modes at a spanwise wavelength of 2.67 mm.

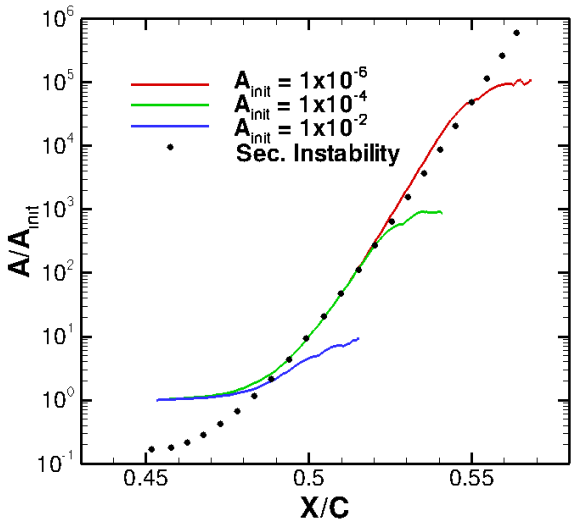

(a) Y-mode of secondary instability, f = 52.5 kHz.

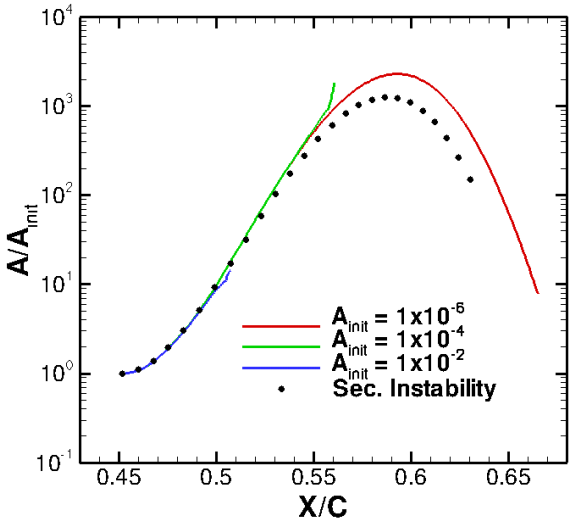

(b) Z-mode of secondary instability, f = 42.5 kHz.

Figure 7. RMS amplitude evolution of chordwise velocity fluctuations

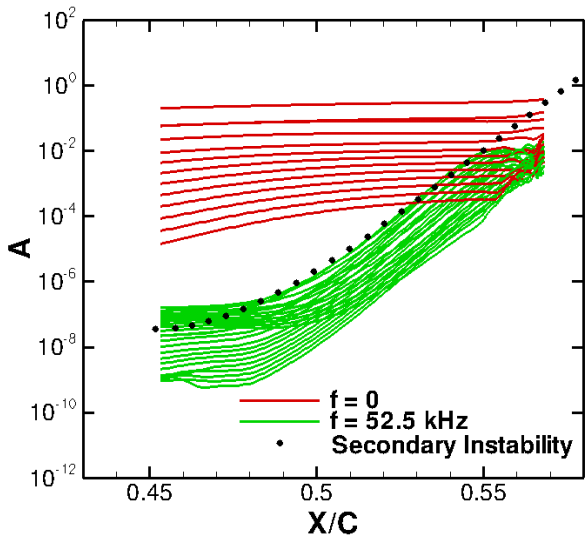

(a) Y-mode of secondary instability

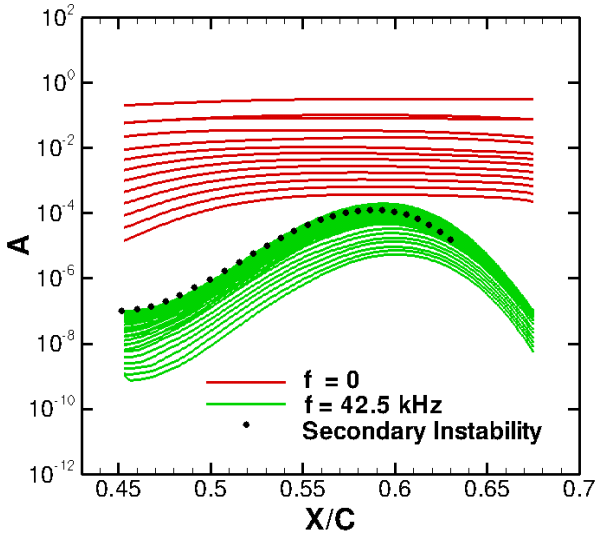

(b) Z-mode of secondary instability

Figure 8. Modal amplitude evolution of primary (red curves) and secondary instability (green curves) based on nonlinear PSE. Dotted lines indicate predictions from PDE based eigenvalue analysis for secondary instability

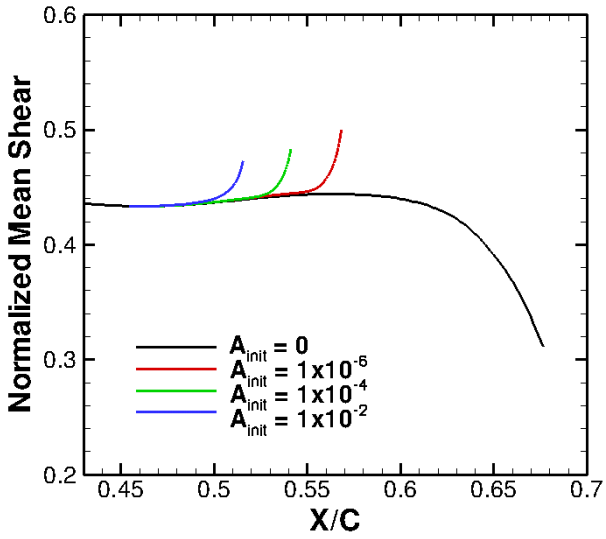

(a) Y-mode of secondary instability

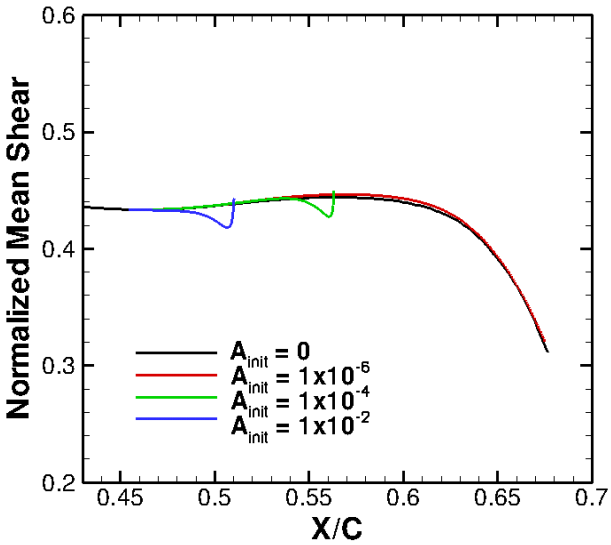

(b) Z-mode of secondary instability

Figure 9. Wall shear evolution resulting from nonlinear evolution of secondary instability modes.

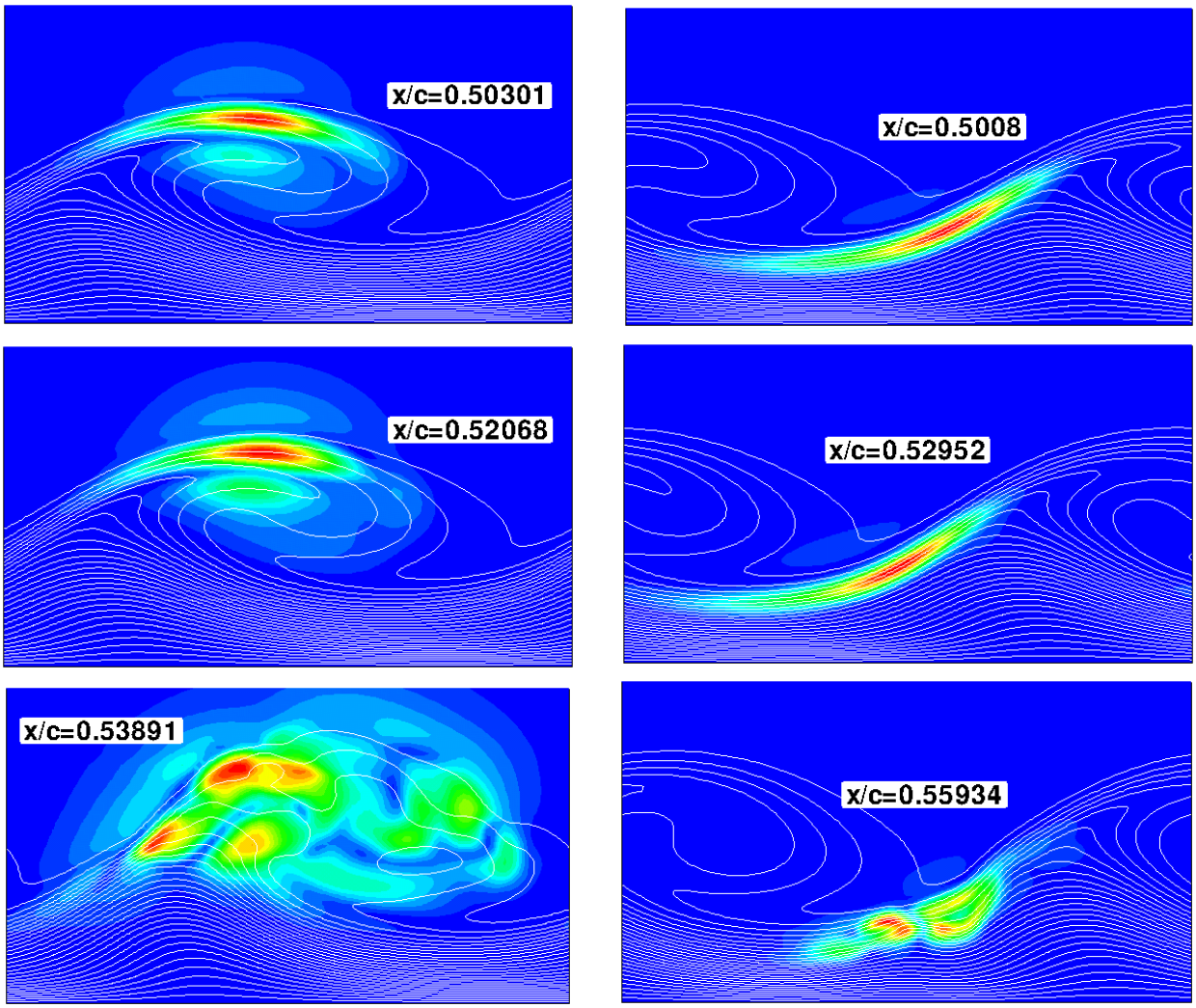

(a) Y-mode. (b) Z-mode.

Figure 10. Time-RMS distributions of chordwise velocity at selected chordwise stations during the nonlinear evolution. The white lines in the background are the u-contours of stationary crossflow vortex. The y-mode is displayed on the left and the z-mode on the right. Secondary instability initial amplitude is 10^{-4} for both modes. In both figures, the horizontal extent of the figure corresponds to a single spanwise wavelength of the stationary crossflow modes (*i.e.* 8 mm in the present case).

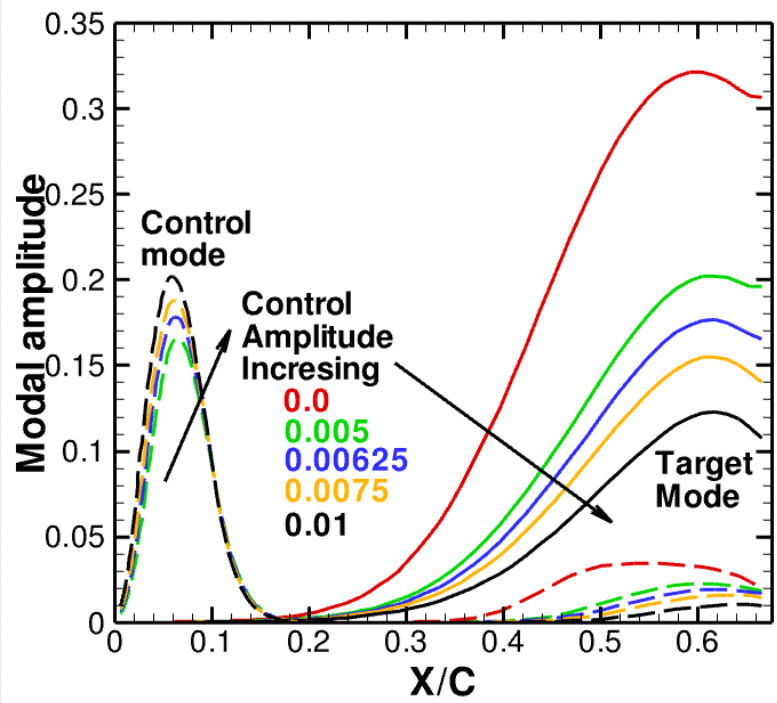

Figure 11. Amplitude evolution of 8mm target mode (solid lines) in the presence of 2.67mm control input at various initial amplitudes (dashed lines). Initial amplitude of the target mode is held fixed at 10^{-5}. Arrows indicate the progressive reduction in target mode amplitude as the control amplitude is increased.

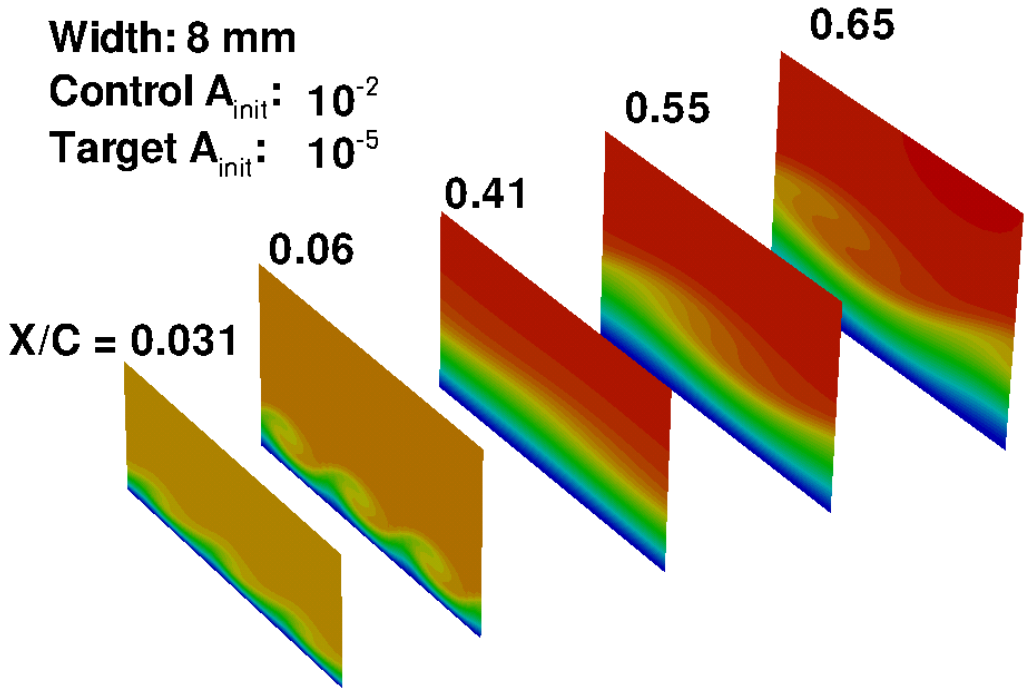

Figure 12. Chordwise velocity contours at 5 constant X/C planes. Control mode of 2.67 mm grows close to the leading edge followed by the emergence of 8mm target mode in the downstream region. Each plane has a width of 8 mm.

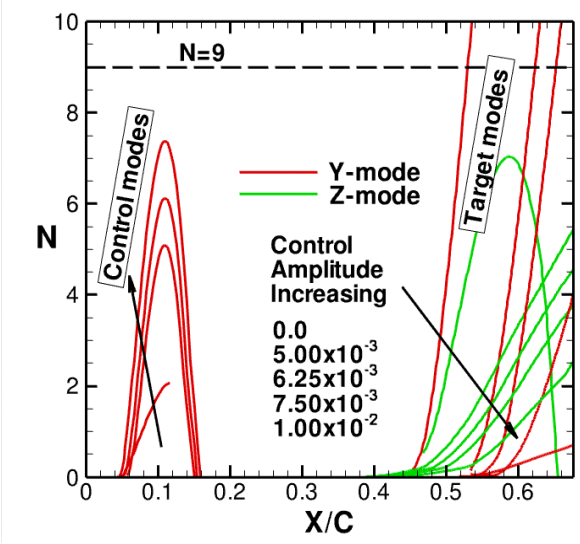

Figure 13. Envelopes of N-factor curves for secondary instability modes for combined evolution of target and control modes. Curves on the left represent N-factors attained by secondary instability of the 2.67 mm control mode. The maximum N factor for the largest control mode amplitude of 10^{-2} is below 8. Curves on the right denote the N-factors attained by secondary instability of the basic state dominated by the 8mm target mode. With a large enough control amplitude, the target mode N-factors become sufficiently small that transition due to breakdown of 8 mm crossflow vortex becomes highly unlikely.

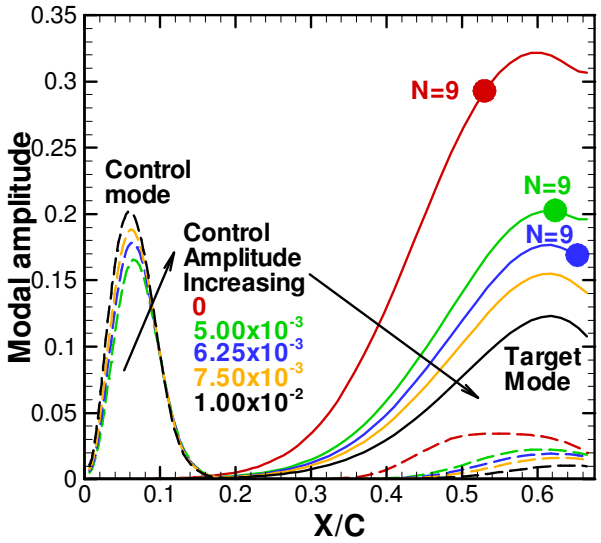

Figure 14. Same as Fig. 11, with the addition of transition locations estimated on the basis of secondary N-factor predictions from Fig. 13. The round dots indicate where secondary instability first reaches an N-factor of 9.

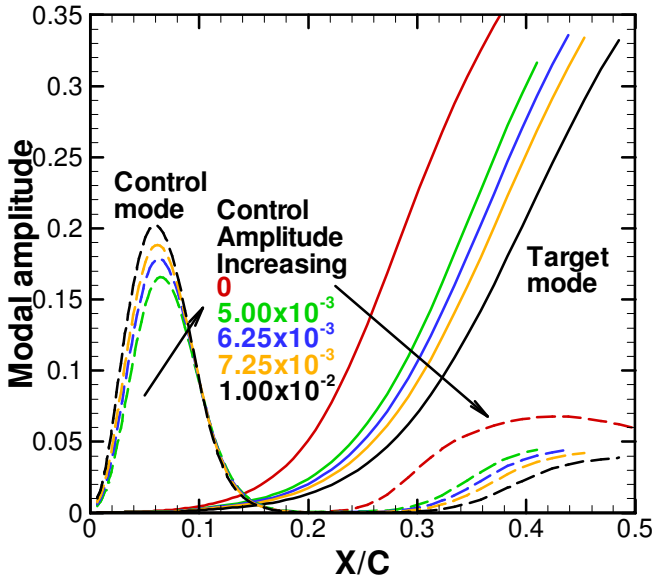

Figure 15. Effect of 2.67mm control input (dashed lines) on the amplitude evolution of 8mm target mode with an initial amplitude of 10^{-4} (solid lines), 10 time larger than that shown in Fig. 14. Arrows indicate the progressive reduction in target mode amplitude as the control amplitude is increased.

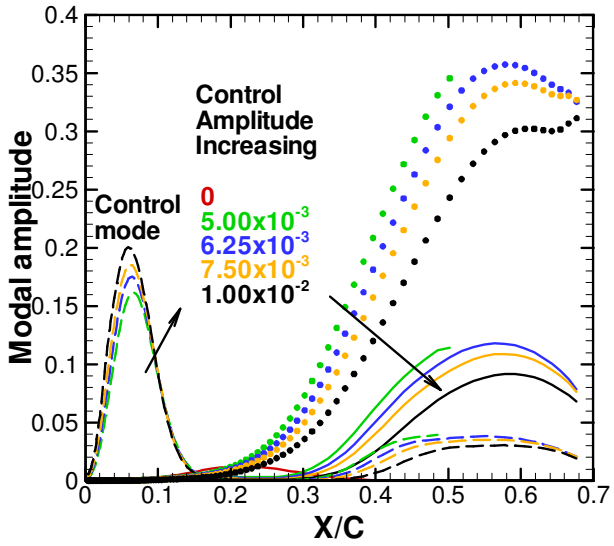

Figure 16. Effect of 2.67mm control input (dashed lines) on 4mm target mode (solid lines). Initial amplitude of the target mode is held fixed at 10^{-5}. Solid dots indicate the amplitudes of 8 mm mode excited via difference interaction between the target and control modes. Arrows indicate the progressive reduction in target mode amplitude as the control amplitude is increased.

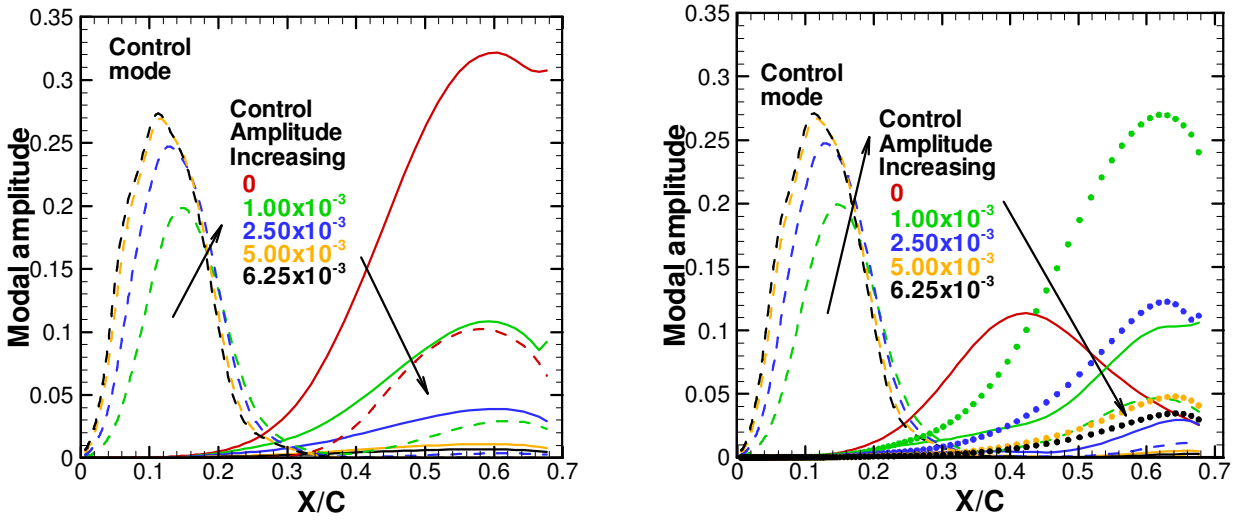

(a) Target mode: λ = 8 mm (b) Target mode: λ = 6 mm

Figure 17. Effect of 4 mm control input (dashed lines) on 8 mm and 6 mm target modes (solid lines). Initial amplitude of the target mode is held fixed at 10^{-5}. Solid dots indicate the amplitudes of 12 mm mode excited via difference interaction between the target and control modes. Arrows indicate the progressive reduction in target mode amplitude as the control amplitude is increased.

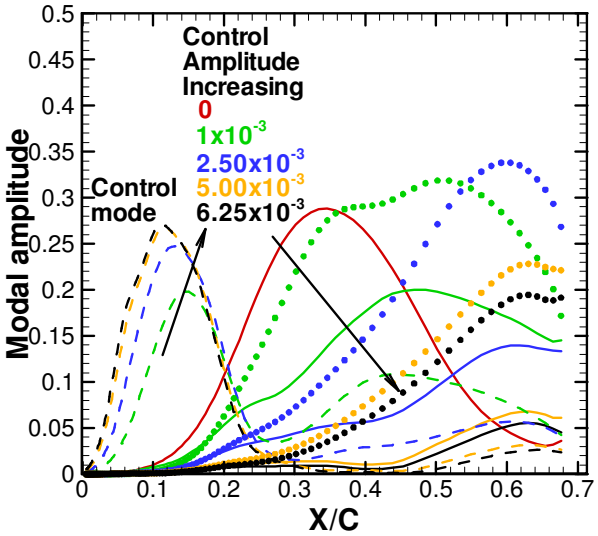

Figure 18. Effect of 4 mm control input (dashed lines) on the amplitude evolution of 6 mm target mode with an initial amplitude of 10^{-4} (solid lines), 10 than larger than that shown in Fig. 17 (b). Arrows indicate the progressive reduction in target mode amplitude as the control amplitude is increased. Solid dots indicate the amplitudes of 12 mm mode excited via difference interaction between the target and control modes.